A twodimensional ion kinetic model of the scrapeoff layer of a diverted plasma with a private flux region

Peter J. Catto and J. W. Connor

Citation: Phys. Plasmas 2, 218 (1995); doi: 10.1063/1.871093
View online: http://dx.doi.org/10.1063/1.871093
View Table of Contents: http://pop.aip.org/resource/1/PHPAEN/v2/i1
Published by the American Institute of Physics.

Related Articles

Free boundary ballooning mode representation
Phys. Plasmas 19, 102506 (2012)

Resistive and ferritic-wall plasma dynamos in a sphere
Phys. Plasmas 19, 104501 (2012)

Plasma flows in scrape-off layer of Aditya tokamak
Phys. Plasmas 19, 092507 (2012)

Self consistent radio-frequency wave propagation and peripheral direct current plasma biasing: Simplified three dimensional non-linear treatment in the “wide sheath” asymptotic regime
Phys. Plasmas 19, 092505 (2012)

Influence of equilibrium shear flow on peeling-ballooning instability and edge localized mode crash
Phys. Plasmas 19, 092503 (2012)

Additional information on Phys. Plasmas

Journal Homepage: http://pop.aip.org/

Journal Information: http://pop.aip.org/about/about_the_journal

Top downloads: http://pop.aip.org/features/most_downloaded

Information for Authors: http://pop.aip.org/authors

ADVERTISEMENT

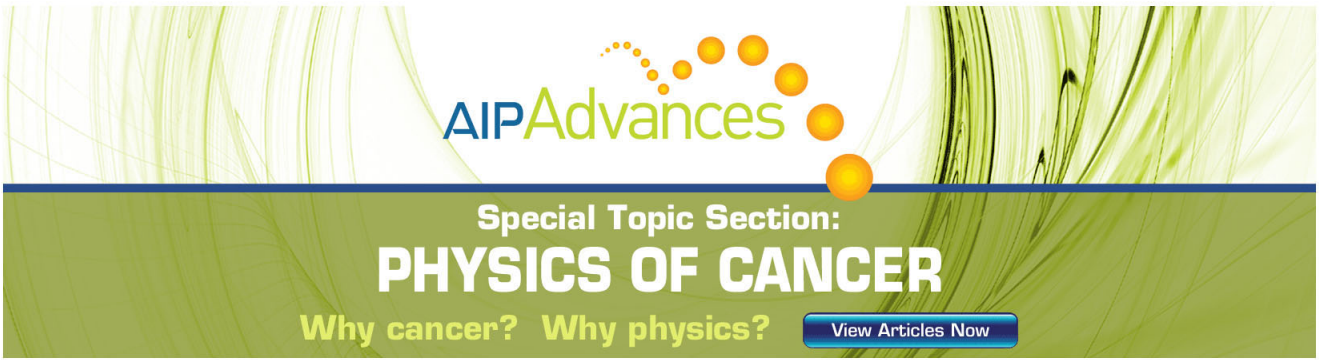

Downloaded 31 Oct 2012 to 194.81.223.66. Redistribution subject to AIP license or copyright; see http://pop.aip.org/about/rights_and_permissions

A two-dimensional ion kinetic model of the scrape-off layer of a diverted plasma with a private flux region

Peter J. Catto
Massachusetts Institute of Technology, Plasma Fusion Center, 167 Albany Street, NW16-236, Cambridge, Massachusetts 02139

J. W. Connor
UKAEA Government Division, Fusion (Euratom/UKAEA Fusion Association), Culham, Abingdon, Oxfordshire, OX143DB, United Kingdom

(Received 22 July 1994; accepted 3 October 1994)

Earlier two-dimensional (radial and poloidal angle), analytically tractable ion kinetic models of the scrape-off layer (SOL) in which a steady state is achieved by balancing the streaming loss of ions to the divertor target plates with the radial diffusion of ions from the core are unable to distinguish between limited and diverted plasmas. The model presented here removes this limitation while still remaining amenable to a similar Wiener–Hopf solution procedure. To phenomenologically model ion recycling, the boundary conditions employed at the divertor plates allow for partial reflection. The diffusion into the private flux region and the extended divertor channels (all of normalized length d along the magnetic field), as well as the rest of the SOL, is evaluated. The SOL is shown to be asymmetric about the separatrix because ions from the core must stream by the X point before diffusing into the private flux region. The channel or leg SOL width is of order $[LD(1+2d)/v_i\,|\ln\gamma|]^{1/2}$, where D, L, v_i, and γ are the diffusion coefficient, connection length, ion thermal speed, and reflection coefficient, respectively. The SOL in the private flux region is narrower (by $[2d/(1+2d)]^{1/2}$) with a lower density (by $[2d/(1+2d)]^{3/4}$) and a stronger poloidal dependence than the region beyond the separatrix. To equalize the heat load between the private flux region and the leg portions of the target, the legs must be longer than the connection length. © *1995 American Institute of Physics.*

I. INTRODUCTION

To control contact between the confined hot plasma within the last closed flux surface and the vessel wall, tokamaks use either a limiter or a divertor to form a scrape-off layer[1] (SOL). In the SOL, located in the vicinity of the last closed flux surface, the radial diffusion from the core is abruptly converted to parallel streaming to the limiter or divertor plates so that two-dimensional models become necessary. By employing a separatrix in the poloidal magnetic field to define the last closed flux surface, divertors are able to ensure that particle and power flows to material walls occur in regions isolated from the hot core plasma. The separatrix results in a private flux region not present in limited plasmas. The private flux region is accessible to particles from the core that are streaming towards the divertor plates and have passed by the null point if they then diffuse back across the separatrix. To distinguish a diverted plasma from a limited one it is necessary to model the private flux region. Existing analytically tractable kinetic models of the ions in the SOL[2–4] do not attempt to model the private flux region. The purpose of this work is to remove this deficiency by solving an analytically tractable two-dimensional ion kinetic model that retains the essential features of a divertor including the private flux region. All ion kinetic models, including the one considered here, are long, mean-free path models in the sense that ion collisions in the scrape-off layer are either neglected entirely or enter only via their effect on spatial diffusion. Long, mean-free path ion models are appropriate for present-day tokamaks, and may remain relevant in some reactor operating regimes.

The earliest ion kinetic model of the SOL region[2] employed a spatial diffusion coefficient due to collisions into the finite orbit loss regions in velocity space created by passing ions being lost at perfectly absorbing up–down symmetric walls intended to model a double null divertor. Subsequent ion kinetic models[3,4] permitted the spatial diffusion to be either collisional or anomalous and focused on evaluating particle and heat fluxes to the walls, providing boundary conditions on the core density and temperature gradients, determining the structure of the SOL including its density profile, and, by assuming the electrons to be Maxwell–Boltzmann, the electrostatic potential. A double diffusion electron model[5] improves upon the Maxwell–Boltzmann model by retaining both the radial feed from the core and the velocity space scattering over the electron reflecting Debye sheaths. In both Refs. 2 and 3, perfectly absorbing walls were assumed and the resulting diffusion equation with boundary conditions was mathematically equivalent to that for the distribution function for diffusion into a loss cone in velocity space associated with the magnetic mirror end-loss problem solved by Baldwin, Cordey, and Watson.[6] In later ion work,[4] the perfectly absorbing wall boundary condition is removed by modeling ion recycling at the walls by an effective reflection coefficient. The ion distribution function in the outer part of the SOL is found to be altered by even a small reflection coefficient. Not only does the SOL widen as expected, but its radial dependence changes unless the reflection coefficient

 1070-664X/95/2(1)/218/9/$6.00 © 1995 American Institute of Physics

Downloaded 31 Oct 2012 to 194.81.223.66. Redistribution subject to AIP license or copyright; see http://pop.aip.org/about/rights_and_permissions

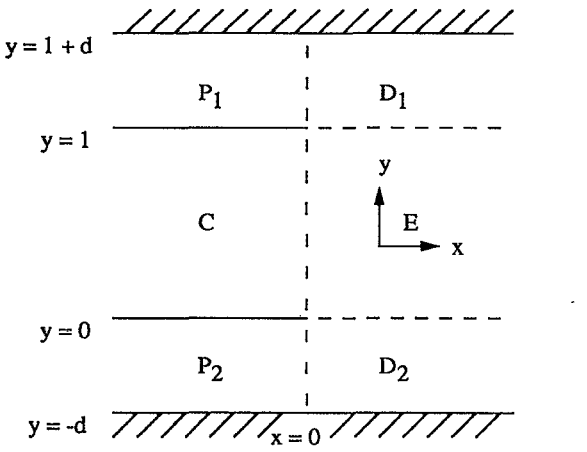

FIG. 1. Schematic of the simplified Cartesian divertor geometry with a private flux region with $x=0$ corresponding to the separatrix. The target plates are denoted by cross-hatching.

becomes vanishingly small. While the recycling model of Helander and Catto[4] is obviously an oversimplication, it will be adopted for our divertor model which includes a private flux region, since it is a substantial improvement over the perfectly absorbing models used in the earlier work. In the model of Ref. 4 ions stream along the magnetic field to the divertor plates where they recombine, reflect, or are absorbed. The neutrals that result from recombination move away from the wall undergoing charge exchange until they ionize. The resulting ions are then assumed to stream back along the magnetic field at the same energy as they entered the presheath. The effective recycling or reflection coefficient γ, which must be such that $0 \leqslant \gamma < 1$, broadens the SOL width by $\sim |\ln \gamma|^{-1/2}$.

The simplified Cartesian divertor model adopted in this paper is the one used in fluid simulations to retain the essential features of the private flux region.[7] It ignores the geometric complications of a spatially varying magnetic field and toroidal geometry. Figure 1 illustrates the Cartesian models relation to a typical single null divertor. In the Cartesian model $x=0$ corresponds to the separatrix, with the core (C) and two private flux regions (P_1 and P_2) at $x<0$, and the edge (E) and two divertor leg or channel regions (D_1 and D_2) at $x>0$. In a single null divertor there is only one private flux region. As a result, the boundary conditions on the two private flux regions of the Cartesian model must be chosen to make them behave as a single region. Such a specification is accomplished by demanding that whatever enters or leaves the lower private flux region via the boundary at $y=0$ emanates from or reappears at the boundary of the upper private flux region at $y=1$; that is, we demand that $y=0$ and $y=1$ be the same line for $x<0$ and that the ion distribution function be continuous across it. The $x>0$ regions D_1 and D_2, above $y=1$ and below $y=0$, correspond to the extended divertor legs on either side of the private flux region bounded by the separatrix.

For the preceding Cartesian divertor model, a kinetic equation balancing radial transport, which supplies ions from the core, with streaming, which causes ions to be lost to the divertor plates, will be solved. The model retains the essential features of the private flux region in a fully two-dimensional manner for realistic boundary conditions which model recycling by an effective reflection coefficient. The geometrical complications make it necessary to neglect the weak parallel variation of the electrostatic potential and consider the long mean-free-path limit in which collisions are ignored in the SOL.

In Sec. II, the long mean-free-path model equation and the boundary conditions appropriate for the preceding model are discussed. Section III uses a generalization of the Wiener–Hopf method of Ref. 4 to find the formal solution for the ion distribution function everywhere and Sec. IV gives the solution in terms of infinite sums and derives limiting forms for $|x| \gg 1$. Various moments of the ion distribution function are evaluated for a velocity independent diffusivity in Sec. V to determine particle and heat loads on the plates, boundary conditions on the core density and temperature, SOL widths, and asymptotic behaviors far from the separatrix. Section VI is a brief discussion of the new features and modifications due to the private flux region.

II. EQUATION AND BOUNDARY CONDITIONS

In the SOL parallel streaming, spatial diffusion, collisions, and a parallel electric field can influence the ion dynamics. However, Refs. 3 and 4 have shown that for a Maxwell–Boltzmann electron response, the parallel variation of the electrostatic potential Φ is weak except in the immediate vicinity of the intersection of the separatrix with the walls where the strong ion density variation leads to an ion accelerating potential which adds to that due to the Debye sheath. Since this is a highly localized region (although not as localized as the Debye sheath which is assumed infinitely thin), the acceleration that takes place is neglected in order that parallel electric field effects may be dropped in the ion kinetic equation. Moreover, by working in the long mean-free path limit the influence of the ion collision operator in the SOL may be ignored. While a more general treatment of collisions in the SOL is desirable, it has not yet been possible to construct an analytically tractable model. The remaining terms in the ion kinetic equation, parallel streaming to the plates and radial diffusion from the core, must be retained since they provide the loss and source terms for the SOL.

Because of the preceding assumptions only the simplified kinetic equation

$$v_{\parallel} \hat{\mathbf{n}} \cdot \nabla f = r^{-1} \frac{\partial}{\partial r} \left(rD \frac{\partial f}{\partial r} \right) \tag{1}$$

needs to be considered, where f is the ion distribution function, r a generalized minor radius variable equal to a at the separatrix, $\hat{\mathbf{n}} = \mathbf{B}/B$ a unit vector along the magnetic field $\mathbf{B}$ with $B = |\mathbf{B}|$, $v_{\parallel} = \hat{\mathbf{n}} \cdot \mathbf{v}$ the parallel ion velocity, and D the spatial diffusion coefficient. Following Refs. 3 and 4, we do not specify the mechanism giving rise to the possibly velocity dependent radial diffusion coefficient D. It may be assumed to be Bohm-like or due to some anomalous process

Downloaded 31 Oct 2012 to 194.81.223.66. Redistribution subject to AIP license or copyright; see http://pop.aip.org/about/rights_and_permissions

giving rise to an alternate form. If D is due to classical or neoclassical collisions then it can be obtained from the Fokker–Planck collision operator by a gyrokinetic change of variables. If D arises because of collisional scattering into velocity space loss regions it can be constructed by the procedure of Hinton and Hazeltine.[2]

To obtain the desired form of the ion kinetic equation we first introduce a generalized poloidal angle variable θ, where $\hat{\mathbf{n}}\cdot\nabla\theta = 1/qR$ with q and R the safety factor and major radius. Inside the separatrix ($r<a$), we take $0<\theta<2\pi$ in the core and $\theta<0$ and $\theta>2\pi$ for the private flux region. Outside the separatrix ($r>a$) we take $0<\theta<2\pi$ in the edge, and $\theta<0$ and $\theta>2\pi$ for the extended divertor channels. Then we introduce the normalized poloidal and radial variables

$$y=\theta/2\pi \quad \text{and} \quad x=(r-a)(|v_\parallel|/LD)^{1/2} \tag{2}$$

with $L=2\pi qR$ the connection length, to write the ion kinetic equation in the form

$$\sigma\frac{\partial f_\sigma}{\partial y}=\frac{\partial^2 f_\sigma}{\partial x^2}, \tag{3}$$

where $\sigma=v_\parallel/|v_\parallel|$ and

$$f=\begin{cases} f_+(x,y) & v_\parallel>0, \\ f_-(x,y) & v_\parallel<0. \end{cases} \tag{4}$$

The y variable is defined such that $0<y<1$ in the core ($x<0$) and the edge ($x>0$). The private flux region ($x<0$) and the divertor channels ($x>0$) correspond to $-d<y<0$ and $1<y<1+d$, where d is the normalized depth of the private flux region and extended divertor legs or channels.

Our constant magnetic field model implies a symmetry about $\theta=\pi$ giving the symmetry condition

$$f_{-\sigma}(x,y)=f_\sigma(x,1-y) \tag{5}$$

about $y=1/2$. As a result, we need only find the solution for $f_+(x,y)$ to find f everywhere.

Equation (3) must be solved in the simplified Cartesian divertor model with boundary conditions corresponding to a steady-state solution in which particles lost to the target plates are resupplied via diffusion from the core. To allow for a radial flux from the core into the SOL we must have

$$f_+(x\to-\infty,0<y<1)\to\alpha+\beta x, \tag{6a}$$

with the velocity space dependent quantities α and β independent of x and y. In order that the core be periodic we require

$$f_+(x<0,y=1-\delta)=f_+(x<0,y=\delta), \tag{6b}$$

where $\delta>0$ and is infinitesimally small. Demanding that whatever leaves (enters) the lower portion of the split private flux region at $y=0$ reappears at (disappears from) the upper portion at $y=1$ gives

$$f_+(x<0,y=1+\delta)=f_+(x<0,y=-\delta). \tag{6c}$$

Assuming that there are no sources in the private flux region and that ions can only be lost to the divertor plates means that f_+ must vanish far from the separatrix giving

$$f_+(x\to-\infty,-d<y<0 \quad \text{and} \quad 1<y<1+d)\to 0. \tag{6d}$$

Beyond the separatrix there are no sources and ions can only be lost to the plates so that

$$f_+(x\to\infty,-d<y<1+d)\to 0. \tag{6e}$$

Finally, we must impose the reflecting boundary condition at the plates. At the top plate the distribution of particles leaving the plate must equal the reflection coefficient times the particles entering the top plate, $f_-(x,y=1+d)=\gamma f_+(x,y=1+d)$. Using the symmetry condition gives the effective recycling or reflecting boundary condition at the plates to be

$$f_+(x,y=-d)=\gamma f_+(x,y=1+d) \tag{6f}$$

for all x. In the next section we solve Eq. (3) for the set of boundary conditions of Eqs. (6) using a Wiener–Hopf procedure.

III. SOLUTION TECHNIQUE

To solve Eq. (3) with the boundary conditions (6) for f_+ it is convenient to introduce the transform pair

$$F_+(k,y)=\int_{-\infty}^{\infty}dx\, f_+(x,y)\exp(ikx)$$

and (7)

$$f_+(x,y)=(2\pi)^{-1}\int_{-\infty}^{\infty}dk\, F_+(k,y)\exp(-ikx).$$

In transform space Eq. (3) becomes

$$\frac{\partial F_+}{\partial y}=-k^2F_+ \quad \text{or} \quad F_+(k,y)\exp(k^2y)$$

$$=\text{constant independent of } k \text{ and } y. \tag{8}$$

Next, we define the following four analytic functions:

$$L(k)=\int_{-\infty}^{0}dx\, f_+(x,y=1-\delta)\exp(ikx)$$

$$=\int_{-\infty}^{0}dx\, f_+(x,y=\delta)\exp(ikx), \tag{9a}$$

$$U(k)=\int_{0}^{\infty}dx\, f_+(x,y=1)\exp(ikx), \tag{9b}$$

$$A(k)=\int_{0}^{\infty}dx\, f_+(x,y=0)\exp(ikx), \tag{9c}$$

and

$$B(k)=\int_{-\infty}^{0}dx\, f_+(x,y=1+\delta)\exp(ikx)$$

$$=\int_{-\infty}^{0}dx\, f_+(x,y=-\delta)\exp(ikx), \tag{9d}$$

where k is restricted to provide convergence. To make $L(k)$ an analytic function the asymptotic behavior given by Eq. (6a) requires that k be below the real k axis. The functions $U(k)$ and $A(k)$ are analytic for k above and slightly below the real k axis, since f_+ must satisfy Eq. (6e). To satisfy Eq.

Downloaded 31 Oct 2012 to 194.81.223.66. Redistribution subject to AIP license or copyright; see http://pop.aip.org/about/rights_and_permissions

(6d), $B(k)$ is analytic for k below and slightly above the real k axis. In addition to the preceding functions, we define

$$H(k)=F_+(k,y=1+d) \tag{9e}$$

which because of the reflecting boundary condition (6f) gives

$$F_+(k,y=-d)=\gamma H(k). \tag{9f}$$

Using the preceding definitions and Eq. (8) we can obtain three equations relating U, L, A, B, and H. For $0<y<1$ we find

$$L+A=(L+U)\exp(k^2). \tag{10a}$$

Similarly, $1<y<1+d$ gives

$$B+U=H\ \exp(k^2d), \tag{10b}$$

while $-d<y<0$ yields

$$B+A=\gamma H\ \exp(-k^2d). \tag{10c}$$

Eliminating H from Eqs. (10) and rewriting gives the two equations,

$$L=-A-\{(U-A)/[1-\exp(-k^2)]\}$$

and (11)

$$B=-U+\{(U-A)/[1-\gamma\ \exp(-2k^2d)]\},$$

which may be subtracted to find

$$-(U-A)/(L-B)=V(k), \tag{12}$$

where V is defined as

$$V(k)=\{[1-\exp(-k^2)][1-\gamma\ \exp(-2k^2d)]\}/\{1-\gamma\ \exp[-(1+2d)k^2]\}. \tag{13}$$

The important point about the form of Eq. (12) is that $U-A$ is an analytic function above and slightly below the real k axis, while $L-B$ is an analytic function below the real k axis. This is the key observation that allows the technique of Ref. 4 to be employed in the more complicated geometry of Fig. 1.

If we arrange the zeroes of the denominator and numerator of V such that

$$V(k)=V_L(k)/V_U(k) \tag{14}$$

with $V_L(k)$ analytic below the real k axis and $V_U(k)$ analytic above and slightly below the real k axis then we can define an entire function C via

$$C=\begin{cases}(L-B)V_L & \text{below real } k \text{ axis,}\\ -(U-A)V_U & \text{above and slightly below real } k \text{ axis.}\end{cases} \tag{15}$$

Integration by parts gives U, L, B, and $A\to O(1/k)$ as $|k|\to\infty$. Therefore, if we arrange for V_L, $V_U\to O(k)$ as $|k|\to\infty$, then Liouville's theorem tells us that any bounded, entire function is necessarily a constant so it must be that

$$C=\text{const.} \tag{16}$$

As a result,

$$L-B=C/V_L \quad \text{and} \quad U-A=-C/V_U, \tag{17}$$

which in combination with Eqs. (11) gives $L+U=F_+(k,y=1-\delta)$, $B+A=F_+(k,y=-\delta)$, and $B+U=F_+(k,y=1+\delta)$ in terms of V_U or V_L.

For $0<y<1$ we may employ $F_+(k,y)\exp(k^2y)=(L+U)\exp(k^2)$ to find the two forms,

$$F_+(k,y)=C\ \exp(-k^2y)/\{V_U[1-\exp(-k^2)]\} \tag{18a}$$

$$=C\ \exp(-k^2y)[1-\gamma\ \exp(-2k^2d)]/\{V_L[1-\gamma\ \exp(-k^2-2k^2d)]\}. \tag{18b}$$

Similarly, when $1<y<1+d$ we use $F_+(k,y)\exp(k^2y)=(B+U)\exp(k^2)$ to find the two forms

$$F_+(k,y)=-C\ \exp(k^2-k^2y)/\{V_U[1-\gamma\times\exp(-2k^2d)]\} \tag{19a}$$

$$=-C\ \exp(k^2-k^2y)[1-\exp(-k^2)]/\{V_L[1-\gamma\ \exp(-k^2-2k^2d)]\}. \tag{19b}$$

Finally, the last set of forms is for $-d<y<0$ where we use $F_+(k,y)\exp(k^2y)=(B+A)$ to find

$$F_+(k,y)=-\gamma C\ \exp(-2k^2d-k^2y)/\{V_U[1-\gamma\times\exp(-2k^2d)]\} \tag{20a}$$

$$=-\gamma C\ \exp(-2k^2d-k^2y)[1-\exp(-k^2)]/\{V_L[1-\gamma\times\exp(-k^2-2k^2d)]\}. \tag{20b}$$

Because of the analytic properties of V_U and V_L, the forms (18a), (19a), and (20a) are convenient above and slightly below the real k axis, while (18b), (19b), and (20b) are convenient in the lower half-k plane.

By inserting Eqs. (18)–(20) into Eq. (7) a transform representation of the solution for $f_+(x,y)$ is obtained for all x and y once the V_L and V_U of Eq. (14) are made explicit. A convenient form of this so-called factorization (which is not unique) is a generalization of that used in Ref. 4, namely

$$V_U(k)=(k+i\sigma)\exp[-q_U(k)]$$

and (21)

$$V_L(k)=[k^2/(k-i\sigma)]\exp[-q_L(k)]$$

with $\sigma>0$ and arbitrary,

$$q_{U,L}(k)=(2\pi i)^{-1}\int_{-\infty\mp i\delta}^{\infty\mp i\delta}dz\ q(z)/(z-k) \tag{22}$$

and

$$q(z)=\ln\{(z^2+\sigma^2)[1-\exp(-z^2)][1-\gamma\times\exp(-2z^2d)]/z^2[1-\gamma\ \exp(-z^2-2z^2d)]\}, \tag{23}$$

where here and in the following the upper signs are to be used with q_U and the lower with q_L unless otherwise noted. Notice that σ is introduced to make the logarithm in Eq. (23) analytic in a strip about the real k axis so Cauchy's theorem can be used to find

$$q(k)=q_U(k)-q_L(k). \tag{24}$$

Downloaded 31 Oct 2012 to 194.81.223.66. Redistribution subject to AIP license or copyright; see http://pop.aip.org/about/rights_and_permissions

An extension of the procedure used in Ref. 4 is used to find an alternate form of Eq. (22) in terms of the Riemann zeta function

$$\zeta(s)=\sum_{n=1}^{\infty} n^{-s} \quad (\mathrm{Re}\ s>1) \tag{25a}$$

and polylogarithm function[8]

$$\phi(s,\gamma)=\sum_{n=1}^{\infty} \gamma^n/n^s \quad (\mathrm{Re}\ s>0, |\gamma|<1), \tag{25b}$$

where $\phi(s,1)=\zeta(s)$ for $\mathrm{Re}\ s>1$, but suitable analytic continuations must be employed for other values of s, as shown in the Appendix therein and in Ref. 9. The resulting expression is

$$q_{U,L}(k)=\pi i/2 \pm \ln(\mp i\sigma - k) \mp S_{\pm}(k,d,\gamma) \tag{26}$$

with

$$S_{\pm}(k,d,\gamma)=\sum_{n=1}^{\infty} \frac{(\pm ik)^n}{n\Gamma(n/2)} \{\zeta(1-n/2)-[(1+2d)^{n/2} - (2d)^{n/2}]\phi(1-n/2,\gamma)\}, \tag{27}$$

where the details of obtaining this alternate form are presented in Appendix A. In Eq. (27), $\phi(s,1)\neq\zeta(s)$ because $\mathrm{Re}\ s\leqslant 1$. Using Eq. (24) we find

$$S_+ + S_- = \ln\{k^2[1-\gamma \exp(-k^2-2k^2d)]/[1 - \exp(-k^2)][1-\gamma \exp(-2k^2d)]\}. \tag{28}$$

In the difference only the odd terms in the sum contribute allowing us to write

$$S_+ - S_- = \sum_{n=0}^{\infty} \frac{(ik)^{2n+1}}{\Gamma(n+\frac{3}{2})} - \left[\zeta\left(\frac{1}{2}-n\right) - [(1+2d)^{n+1/2} - (2d)^{n+1/2}]\phi\left(\frac{1}{2}-n,\gamma\right)\right]. \tag{29}$$

Consequently, Eq. (26) may also be rewritten by using $S_{\pm}=[(S_+ + S_-) \pm (S_+ - S_-)]/2$, and these results employed to obtain

$$q_{U,L}(k=0)=\pi i/2 \pm \ln(\mp i\sigma) \tag{30a}$$

and

$$\left.\frac{\partial q_{U,L}(k)}{\partial k}\right|_{k=0} = (i\sigma)^{-1} + i\eta, \tag{30b}$$

where $\zeta(1/2)=-1.46$ and

$$\eta=\pi^{-1/2}\{[(1+2d)^{1/2}-(2d)^{1/2}]\phi(1/2,\gamma)-\zeta(1/2)\}. \tag{30c}$$

The expression for η simplifies for $\gamma\ll 1$, since $\phi(1/2,\gamma)\to\gamma$, and for $\gamma\to 1$ for which[9] $\phi(1/2,\gamma)\to[\pi/(1-\gamma)]^{1/2}$.

In the next section we use the preceding results to verify that our solution satisfies the boundary conditions and to obtain explicit expressions for its large $|x|$ behavior.

IV. LIMITING FORMS OF THE SOLUTION

The transforms $F_+(k,y)$ given by Eqs. (18)–(20) can be inverted to find the solution $f_+(x,y)$ by summing over the residues. This procedure is most useful for finding the large $|x|$ asymptotic form of the solution. For $x<0$, Eqs. (18a), (19a), and (20a) are employed because V_U is analytic above [where $\exp(-ikx)$ provides convergence] and slightly below the real k axis; while for $x>0$ we use Eqs. (18b), (19b), and (20b) because V_L is analytic below with $\exp(-ikx)$ providing convergence.

We consider $x<0$ and $0<y<1$ first by employing Eq. (18a) which has a double pole at $k_0=0$ and single poles at $k_n=[(n/|n|)+i](\pi|n|)^{1/2}$ in the upper half-plane ($n=\pm 1$, ± 2, ± 3...). Remembering that the path of integration must pass below $k=0$ where L and U overlap and extracting the double pole, we find

$$f_+(x,y)=iC\left.\frac{d}{dk}\frac{\exp[-ikx-k^2y+q_U(k)]}{k+i\sigma}\right|_{k=0} + iC\sum_{n=-\infty}^{\infty}\left.\frac{\exp[-ik_nx-k_n^2y+q_U(k_n)]}{2k_n(k_n+i\sigma)}\right|_{n\neq 0} \to -iC(x-\eta)+O[\exp(-\pi^{1/2}|x|)], \tag{31}$$

where Eqs. (30) are employed. Comparison with the boundary condition of Eq. (6a) gives

$$\beta=-iC \quad \text{and} \quad \eta=-\alpha/\beta. \tag{32}$$

Notice that α has been determined in terms of β which means that the scrape-off layer analysis sets the boundary condition on the core gradients[2-4] (in particular, the core density and temperature gradients) and that β is the only x and y independent quantity to be determined.

The velocity dependence of β is chosen by noting that in the core spatial diffusion is weak compared to collisions so that the orbital or bounce average collision operator must vanish to lowest order giving f proportional to a Maxwellian $f_M=N_a(m/2\pi T_a)^{3/2}\exp(-Mv^2/2T_a)$, where N_a and T_a are constants. Equation (31) also requires $|x|\gg 1$ giving $f\propto x\propto|v_\parallel|^{1/2}$ approaching the core. As a result, the choice

$$-\beta=iC=(LD/|v_\parallel|)^{1/2}f_M/l \tag{33a}$$

is employed, so that, recalling (2), the final form of (31) becomes

$$f_+(x,y)\to-(r-a-\eta w_\parallel)f_M/l, \tag{33b}$$

where l is the density scale length approaching the separatrix from the core with N_a/l the density gradient, T_a the temperature, and

$$w_\parallel=(LD/|v_\parallel|)^{1/2}. \tag{33c}$$

The choice of (33a) results in a fixed radial flux from the core, but is not unique. However, a rigorous matching to the core is not available and is beyond the scope of the present treatment. An alternate choice previously employed[2-4] would assume $-\eta\beta$ to be Maxwellian, but it does not make the averaged collision operator vanish towards the core and results in the flux from the core trying to vanish as $\gamma\to 1$.

Downloaded 31 Oct 2012 to 194.81.223.66. Redistribution subject to AIP license or copyright; see http://pop.aip.org/about/rights_and_permissions

Choice (33a) also introduces complications because of its small $v_\parallel$ behavior which results in an infinite number of ions in the SOL, as noted in Ref. 4. However, because the divergent behavior is logarithmic it can be removed by introducing a collisional cutoff at $|v_\parallel|=\nu/L$. Evidently, a rigorous matching must retain collisional effects on the $v_\parallel\to 0$ ions in order to change their parallel velocity so that they can be lost to the plates once they diffuse into the SOL.

Core periodicity, Eq. (6a), is satisfied for $x>0$ because $[1-\exp(-k^2)]^{-1}=1+\{\exp(-k^2)/[1-\exp(-k^2)]\}$ can be used in Eq. (18a) to see that $F_+(k,y=\delta)$ and $F_+(k,y=1-\delta)$ have the same singularities in the upper half-plane.

The behavior of f_+ in the scrape-off layer for $x>0$ and $-d<y<1+d$ is found from Eqs. (18b), (19b), and (20b), all of which have poles at $k_n=\pm\{[-|\ln\gamma|+i2\pi n]/(1+2d)\}^{1/2}$, with the lower (upper) sign giving the poles in the lower (upper) half-plane. Notice that Eqs. (18a), (19a), and (20a) are continuous at $y=0$ and $y=1$ because $1-\gamma\exp(-2k_n^2 d)=1-\exp(k_n^2)=-\gamma\exp(-2k_n^2 d)[1-\exp(-k_n^2)]$. Summing over the poles in the lower half-plane, Eqs. (18b), (19b), and (20b) all result in

$$f_+(x,y)=\frac{\beta}{2(1+2d)}\sum_{n=-\infty}^{\infty}\frac{k_n-i\sigma}{k_n^3}[1-\exp(-k_n^2)]\exp[-ik_n x+k_n^2-k_n^2 y+q_L(k_n)]. \tag{34a}$$

For finite γ we need only keep the pole closest to the real axis, $k_0=-i[|\ln\gamma|/(1+2d)]^{1/2}$. As a result (34) reduces to

$$f_+\to-\frac{\beta(1+2d)^{1/2}}{2|\ln\gamma|^{3/2}}\{1-\exp[-|\ln\gamma|/(1+2d)]\}\times\exp\{S_1-x[|\ln\gamma|/(1+2d)]^{1/2}+y[|\ln\gamma|/(1+2d)]\}, \tag{34b}$$

where $S_q=S_-(\kappa_q,d,\gamma)$ with $\kappa_q=-i[|\ln\gamma|/(q+2d)]^{1/2}$ or

$$S_q=\sum_{n=1}^{\infty}\frac{(-1)^n[|\ln\gamma|/(q+2d)]^{n/2}}{n\Gamma(n/2)}\{\zeta(1-n/2)-[(1+2d)^{n/2}-(2d)^{n/2}]\phi(1-n/2,\gamma)\}\to\ln\left(\frac{(q+2d)^{1/2}+(1+2d)^{1/2}}{(q+2d)^{1/2}+(2d)^{1/2}}\right). \tag{35}$$

The $\gamma\to 1$ form of S_q, given to the right of the arrow in Eq. (35), is derived in Appendix B. In addition to the γ dependence found in Ref. 4, d affects the large x behavior of f_+ by widening the scrape-off layer because of the extra fractional length d of the field line in each divertor channel. The approximation of (34b) only fails for extremely small γ, $|\ln\gamma|^{1/2}\gg 1$, for which additional poles must be retained. In the $\gamma\to 0$ limit we may replace the sum in Eq. (34a) by an integral over $n(\Sigma\to\int dn)$. Changing the variable of integration from n to k_n, deforming the contour well below the real axis, and noting that a saddle point integral can be employed provided $y>0$, gives

$$f_+\to\left(\frac{\beta}{2\pi i}\right)\int_{-\infty}^{\infty}dk\,k^{-1}\exp(-ikx-k^2y)\to-\left(\frac{\beta y^{1/2}}{\pi^{1/2}x}\right)\exp\left(-\frac{x^2}{4y}\right),$$

which is the result of Ref. 3. For $\gamma=0$ the region $-d<y<0$ is not accessible to $v_\parallel>0$ ions giving $f_+=0$, as can be seen from Eq. (20b).

The forms for f_+ in the private flux region are of particular interest, since they show that the scrape-off layer is not symmetric about the separatrix and can be used to find the asymptotic behavior there. Considering $x<0$ and $-d<y<0$ first and summing over the poles $k_n=\pm\{[-|\ln\gamma|+i2\pi n]/2d\}^{1/2}$ in the upper half-plane Eq. (20a) gives

$$f_+(x,y)=\frac{\beta}{4d}\sum_{n=-\infty}^{\infty}\frac{\exp[-ik_n x-k_n^2 y+q_U(k_n)]}{k_n(k_n+i\sigma)}. \tag{36a}$$

Keeping only the pole closest to the real k axis, $k_0=+i(|\ln\gamma|/2d)^{1/2}$, and using $S_+(k_0,d,\gamma)=S_0$, as given by Eq. (35), gives the finite γ result

$$f_+\to\frac{-\beta}{2(2d|\ln\gamma|)^{1/2}}\exp\{-S_0+x(|\ln\gamma|/2d)^{1/2}+y(|\ln\gamma|/2d)\}. \tag{36b}$$

Comparing the x and y dependencies in Eqs. (34b) and (36b) we see that the scrape-off layer width is narrower in the private flux region by $[2d/(1+2d)]^{1/2}$ and the y dependence stronger by $2d/(1+2d)$ because the $v_\parallel>0$ ions can only diffuse into the private flux region once they have passed by the X point ($y=1$). In addition, notice from Eq. (20a) that $f_+=0$ for $\gamma=0$ because $y<0$ is not accessible to $v_\parallel>0$ ions [in this case, an attempt to perform a saddle point evaluation as $\gamma\to 0$ by replacing the sum by an integral in Eq. (36a) fails because there is no saddle in the upper half-plane].

Next, we consider $x<0$ and $1<y<1+d$ by using Eq. (19a) and summing over the poles $k_n=\pm\{[-|\ln\gamma|+i2\pi n]/2d\}^{1/2}$ in the upper half-plane to find

$$f_+(x,y)=\frac{\beta}{4d}\sum_{n=-\infty}^{\infty}\frac{\exp[-ik_n x-k_n^2(y-1)+q_U(k_n)]}{k_n(k_n+i\sigma)}, \tag{37a}$$

which is just (36a) with $y\to y-1$. Therefore, the procedure used to obtain (36b) gives the $-x\gg 1$, finite γ result

$$f_+\to\frac{-\beta}{2(2d|\ln\gamma|)^{1/2}}\exp[-S_0+x(|\ln\gamma|/2d)^{1/2}+(y-1)(|\ln\gamma|/2d)], \tag{37b}$$

again exhibiting the asymmetry of the scrape-off layer about $x=0$. For the limit $\gamma\to 0$, replacing the sum in (37a) by an integral and carrying out the saddle point integral well above the real axis gives

Downloaded 31 Oct 2012 to 194.81.223.66. Redistribution subject to AIP license or copyright; see http://pop.aip.org/about/rights_and_permissions

TABLE I. Summary of asymptotic forms of f_+ for $\gamma=0$ for the regions shown in Fig. 1.

Region in Fig. 1	Asymptotic form of f_+ for $\gamma=0$
C	$f_+\rightarrow\beta\{x-0.824[(1+2d)^{1/2}-(2d)^{1/2}]\}$
E and D_1	$f_+\rightarrow-\beta(y^{1/2}/\pi^{1/2}x)\exp(-x^2/4y)$
P_1	$f_+\rightarrow-\beta[(y-1)^{1/2}/\pi^{1/2}\lvert x\rvert]\exp[-x^2/4(y-1)]$
P_2 and D_2	$f_+=0$

$$f_+\rightarrow(\beta/2\pi i)\int_{-\infty}^{\infty}dk\ k^{-1}\exp[-ikx-k^2(y-1)]$$

$$\rightarrow-[\beta(y-1)^{1/2}/\pi^{1/2}|x|]\exp[-x^2/4(y-1)]. \quad (37c)$$

Comparison with the $\gamma\rightarrow0$ form of (34a) shows that the asymmetry about the separatrix persists even for $\gamma=0$. The effective distance to diffuse for $x<0$ is d giving f_+ an SOL width of $2d^{1/2}$ at $y=1+d$, while for $x>0$ it is $1+2d$ giving a width at $y=1+d$ of $2(1+2d)^{1/2}$. Notice also from (36a) and (37a) that the split private flux region is continuous as required by (6c) since $\exp[k_n^2(1-y)]|_{y=1}=\gamma\exp[-k_n^2(y+2d)]|_{y=0}$ because $1=\gamma\exp(-2k_n^2d)$.

The asymptotic forms of f_+ are summarized in Tables I and II for $\gamma=0$ and $\gamma\rightarrow1$, respectively. To obtain the results shown in the tables the $\gamma=0$ and $\gamma\rightarrow1$ forms of Eq. (30c) and the final form of Eq. (35) are employed.

Based on the asymptotic forms, the normalized scrape-off layer widths associated with the ion distribution function for finite γ are $[(1+2d)/|\ln\gamma|]^{1/2}$ for $x>0$ and $(2d/|\ln\gamma|)^{1/2}$ for $x<0$. The scrape-off width in the private flux region is always smaller than that in the divertor channel because diffusion into the private flux region can only occur once an ion has passed the X point.

Because of the $v_\parallel$ dependence of x, the exponential decay of the ion distribution function in the scrape-off layer results in an algebraic rather than exponential decay in its moments for a $\mathbf{v}$ independent D, as we shall see in the next section. The next section also considers the particle and heat fluxes to the plates and the boundary conditions on the core.

V. MOMENT INFORMATION

In the previous sections, the velocity dependence of D did not need to be specified since it entered as a parameter. In this section we consider various moments of f and in doing so assume that D is independent of $\mathbf{v}$.

The particle (Γ) and power (P) load on the targets can be found by integrating the poloidal particle and heat fluxes,[2-4] $\int d^3v\ fv_\parallel B_P/B_T$ and $\frac{1}{2}M\int d^3v\ fv^2v_\parallel B_P/B_T$, over *both* plates (from $r=-\infty$ to $+\infty$) and multiplying by the circumference $2\pi R$ to find

$$\left.\begin{matrix}\Gamma\\P\end{matrix}\right\}=4\pi R(B_P/B_T)(1-\gamma)\int_{-\infty}^{\infty}dr\int_{v_\parallel>0}$$

$$\times d^3v\left\{\begin{matrix}1\\Mv^2/2\end{matrix}\right\}v_\parallel f_+(x,y=1+d), \quad (38a)$$

where B_P and B_T are the poloidal and toroidal magnetic-field components. The integration is over $v_\parallel>0$, since the recycling condition $f_-(x,y=1+d)=\gamma f_+(x,y=1+d)$ has been inserted. Using $dr=(LD/|v_\parallel|)^{1/2}dx$, $\int_{-\infty}^{\infty}dx\ f_+(x,y=1+d)=H(k=0)=-C/[(1-\gamma)V_U(k=0)]=-\beta/(1-\gamma)$, and Eq. (33a), the integrals can be performed to find

$$\left.\begin{matrix}\Gamma\\P\end{matrix}\right\}=2\pi R(B_PL/B_Tl)DN_a\left\{\begin{matrix}1\\3T_a/2\end{matrix}\right., \quad (38b)$$

where we have used Eqs. (10b), (11), (17), (21), and (26). Notice that the energy carried per particle is $3T_a/2$ (for a half-Maxwellian it is $2T_a$ so the effective flux limit is 3/4) and that D/l is a measure of the plasma flow speed across the separatrix because $B_PL/B_T\approx2\pi r$. The coefficient in (38b) should be viewed with caution, since it is sensitive to the assumed normalization (33a) which is still an active area of research.

The ion density N and temperature T defined by

$$\left.\begin{matrix}N\\3NT/2\end{matrix}\right\}=\int_{v_\parallel>0}d^3v[f_+(x,y)+f_+(x,1-y)]\left\{\begin{matrix}1\\Mv^2/2\end{matrix}\right. \quad (39)$$

can be evaluated asymptotically. In the core region $-x\gg1$ and $0<y<1$, Eqs. (31)–(33a) can be inserted to find

$$\left.\begin{matrix}N\\3NT/2\end{matrix}\right\}=\left[\frac{(a-r)}{l}+\left\{\begin{matrix}1\\5/6\end{matrix}\right\}\frac{\Gamma(1/4)\eta}{(2T_a/M)^{1/4}}\left(\frac{LD}{\pi}\right)^{1/2}\right]$$

$$\times\left\{\begin{matrix}N_a\\3N_aT_a/2\end{matrix}\right.. \quad (40a)$$

Because the scrape-off layer analysis set the boundary condition on the core gradients as found in (31)–(32), the boundary conditions on the core density and temperature gradients are determined as well, as shown by (40a). The density and temperature scrape-off layer widths implied by (40a) are

TABLE II. Summary of asymptotic forms of f_+ for $\gamma\rightarrow1$ for the regions shown in Fig. 1.

Region in Fig. 1	Asymptotic form of f_+ for $\gamma\rightarrow1$
C	$f_+\rightarrow\beta\{x-[(1+2d)^{1/2}-(2d)^{1/2}]/(1-\gamma)^{1/2}\}$
E, D_1, and D_2	$f_+\rightarrow-\beta\lvert\ln\gamma\rvert^{-1/2}[(1+2d)^{1/2}+(2d)^{1/2}]^{-1}\exp\{-x[\lvert\ln\gamma\rvert/(1+2d)]^{1/2}-(y-\frac{1}{2})\ln\gamma/(1+2d)\}$
P_1	$f_+\rightarrow-\beta\lvert\ln\gamma\rvert^{-1/2}[(1+2d)^{1/2}+(2d)^{1/2}]^{-1}\exp\{x[\lvert\ln\gamma\rvert/(2d)]^{1/2}-(y-1)[\ln\gamma/(2d)]\}$
P_2	$f_+\rightarrow-\beta\lvert\ln\gamma\rvert^{-1/2}[(1+2d)^{1/2}+(2d)^{1/2}]^{-1}\exp\{x[\lvert\ln\gamma\rvert/(2d)]^{1/2}-y[\ln\gamma/(2d)]\}$

Downloaded 31 Oct 2012 to 194.81.223.66. Redistribution subject to AIP license or copyright; see http://pop.aip.org/about/rights_and_permissions

$$w \approx \frac{\Gamma(1/4)(LD/\pi)^{1/2}\eta}{(2T_a/M)^{1/4}} \begin{cases} 1 \\ 5/6, \end{cases} \tag{40b}$$

which depend on η and therefore increase with increasing γ because of recycling.

Asymptotic evaluations of the density and temperature can also be carried out in the SOL regions for $-x \gg 1$ and $x \gg 1$. Considering the private flux region for $1<y<1+d$ first, inserting the $-x \gg 1$ forms (36b) with $y \to 1-y$ and (37b) into Eq. (39), defining the private flux region SOL width

$$w_{pf} = \left(\frac{M}{2T_a}\right)^{1/4} \left(\frac{2LDd}{|\ln \gamma|}\right)^{1/2}, \tag{41a}$$

and assuming $|r-a| \gg w_{pf}$, gives

$$\left.\begin{matrix} N \\ 3NT/2 \end{matrix}\right\} \to \frac{N_a(2d)^{1/4}(LD)^{5/4}\cosh[(y-1)\ln \gamma/2d]\exp(-S_0)}{l(2T_a/M)^{5/8}|\ln \gamma|^{5/4}(r-a)^{3/2}} \begin{cases} 1 \\ T_a. \end{cases} \tag{41b}$$

Similarly, outside the separatrix, inserting the $x \gg 1$ form (34b) into (39), defining the leg or edge SOL width

$$w_{\text{leg}} = \left(\frac{M}{2T_a}\right)^{1/4} \left(\frac{LD(1+2d)}{|\ln \gamma|}\right)^{1/2}, \tag{42a}$$

and assuming $(r-a) \gg w_{\text{leg}}$ results in

$$\left.\begin{matrix} N \\ 3NT/2 \end{matrix}\right\} \to \frac{2N_a[LD(1+2d)]^{5/4}\exp(S_1)}{l(2T_a/M)^{5/8}|\ln \gamma|^{9/4}(r-a)^{3/2}} \times \sinh\left(\frac{|\ln \gamma|}{2(1+2d)}\right)\cosh\left(\frac{(2y-1)\ln \gamma}{2(1+2d)}\right)\begin{cases} 1 \\ T_a. \end{cases} \tag{42b}$$

Notice from the form of (41b) and (42b) that the density decays algebraically rather than exponentially and the temperature approaches a constant as $|x| \to \infty$. Moreover, the poloidal dependence in the private flux region is stronger, as can be seen by comparing the cosh terms. The asymmetry about the separatrix in the asymptotic behavior of the density is clearer if we evaluate the ratio of (42b) divided by (41b) at the target:

$$\left.\frac{(42b)}{(41b)}\right|_{y=1+d} \to \left(\frac{1+2d}{2d}\right)^{1/4} \frac{\sinh[\ln\gamma/2(1+2d)]}{[\ln\gamma/2(1+2d)]} \times \exp(S_0+S_1). \tag{42c}$$

For $\gamma \to 1$, the limiting form of (35) gives $\exp(S_0+S_1) \to [(1+2d)/2d]^{1/2}$ so that (42b)/(41b) $\to [(1+2d)/2d]^{3/4}$ rather than the ratio of the total to private flux region field line lengths $(1+2d)/2d$. Finally, as a further measure of the asymmetry of the SOL, note that Eqs. (41a) and (41b) give the characteristic widths of the private flux region and leg regions with $w_{\text{pf}}/w_{\text{leg}} = [2d/(1+2d)]^{1/2} < 1$. Consequently, the legs need to be at least a connection length long to equalize the heat load between the private flux region and leg portions of the target plates.

VI. DISCUSSION

The kinetic behavior of the ions in an idealized two-dimensional divertor model having a private flux region is considered for the first time. This introduces an additional parameter d, the distance from the X point to the target plate normalized by the total length of the field lines just inside the separatrix. The model balances radial diffusion from the core with parallel streaming to recycling target plates, and finds that the divertor legs must be deeper than a connection length to equalize the heat load between the private flux region and leg portions of the target plates.

The ion distribution function and its moments are shown to be asymmetric about the separatrix because ions from the core must diffuse across the separatrix and then stream pass the poloidal field null before they can diffuse into the private flux region. This behavior results in (i) a target SOL width in the private flux region narrower than that beyond the separatrix by $[2d/(1+2d)]^{1/2}$, as found by comparing (34b) and (36b) or (41a) and (42a), (ii) the private flux region density at the target being lower than that beyond the separatrix by roughly $[2d/(1+2d)]^{3/4}$ at the same distance $|x|$ from the separatrix as shown by (42c), and (iii) a stronger poloidal dependence in the private flux region [again compare (34b) and (36b) or (41b) and (42b)], as the density increases towards the target plates, where $d/(1+2d)$ is the length of the field line from the X point to the target plate normalized to the total length of the field line.

The boundary condition on the ion distribution function and its moments [recall (31) and (40a)] depend on d, as well as γ, and recover the limiter $(d \to 0)$ result of Ref. 4. For finite γ and $d \gg 1$, ions from the core are able to diffuse further from the separatrix as they recycle and thereby increase the SOL widths (40b) and (43) to make the transition from the core to the edge less abrupt. The smearing due to the additional diffusion in the private flux region and divertor legs enhances the $\sim|\ln \gamma|^{-1/2}$ spreading from a finite effective ion reflection coefficient γ as can be seen from Eqs. (34b), (36b), and (37b); but does not affect the core boundary conditions for perfectly absorbing walls ($\gamma=0$) as shown by the $\gamma \to 0$ form of (34a) and (37c).

ACKNOWLEDGMENTS

P.J.C. is pleased to acknowledge the hospitality and support of the Theoretical and Strategic Studies Department, UKAEA Government Division, Fusion, at Culham Laboratory, where much of this work was performed.

Downloaded 31 Oct 2012 to 194.81.223.66. Redistribution subject to AIP license or copyright; see http://pop.aip.org/about/rights_and_permissions

This research was jointly supported by U.S. Department of Energy Grant No. DE-FG02-91ER-54109 at the Plasma Fusion Center of the Massachusetts Institute of Technology and the U.K. Department of Trade and Industry and Euratom.

APPENDIX A: ALTERNATE FORM OF $q_{U,L}(k)$

To obtain Eqs. (26) and (27) we generalize the procedure of Ref. 4 by first integrating Eq. (22) by parts to find

$$q_{U,L}(k)=-\frac{1}{\pi i}\int_{-\infty\mp i\delta}^{\infty\mp i\delta}dz\left[\frac{1}{\exp(z^2)-1}+\frac{2\gamma d}{\exp(2z^2d)-\gamma}-\frac{\gamma(1+2d)}{\exp[(1+2d)z^2]-\gamma}-\frac{\sigma^2}{z^2(z^2+\sigma^2)}\right]z\,\ln(z-k) \tag{A1}$$

and then using the expansion $\ln(z-k)=\ln z-\Sigma_1^\infty n^{-1}(k/z)^n$. Evaluating the integrals, as in Ref. 4, we have

$$\frac{\sigma^2}{\pi i}\int_{-\infty\mp i\delta}^{\infty\mp i\delta}\frac{dz\,z\,\ln(z-k)}{z^2(z^2+\sigma^2)}=\pm\ln(\mp i\sigma-k), \tag{A2}$$

$$\frac{\gamma}{\pi i}\int_{-\infty\mp i\delta}^{\infty\mp i\delta}\frac{dz\,z\,\ln z}{\exp(z^2)-\gamma}=\mp\ln(1-\gamma)^{1/2}, \tag{A3}$$

and

$$\frac{\gamma\kappa}{\pi i}\int_{-\infty\mp i\delta}^{\infty\mp i\delta}\frac{dz\,z^{1-n}}{\exp(\kappa z^2)-\gamma}=\mp\frac{(\pm i\kappa^{1/2})^n}{\Gamma(n/2)}\,\phi(1-n/2,\gamma), \tag{A4}$$

which can be used to obtain Eqs. (26) and (27). When $\gamma=1$ the polylogarithm function on the right side of Eq. (A4) must be replaced by the Riemann zeta function. However, $\phi(1-n/2,\gamma=1)\neq\zeta(1-n/2)$ for $n\geq 0$ because the integrand in (A4) has a singularity at $z=0$ for $\gamma=1$, but not for $\gamma<1$.

APPENDIX B: ASYMPTOTIC EVALUATION OF S_q

The $\gamma\to 1$ form of S_q given in the second form of Eq. (35) is obtained by using[9]

$$\lim_{\gamma\to 1}\left(\frac{\phi(1-n/2,\gamma)}{\gamma}-\frac{\Gamma(n/2)}{\gamma|\ln\gamma|^{n/2}}\right)=\zeta(1-n/2), \tag{B1}$$

to rewrite it as

$$S_q\to\sum_{n=1}^{\infty}\frac{(-1)^n}{n}\left(\frac{(2d)^{n/2}}{(q+2d)^{n/2}}-\frac{(1+2d)^{n/2}}{(q+2d)^{n/2}}\right)+O(|\ln\gamma|^{1/2}). \tag{B2}$$

To evaluate the sum in (B2), we use $1/n=\int_1^\infty dx/x^{n+1}$ to rewrite it as

$$\sum_{n=1}^{\infty}\frac{(-1)^n}{nk^n}=\int_1^\infty\frac{dx}{x}\left(\sum_{n=0}^{\infty}\left(\frac{-1}{kx}\right)^n-1\right)=\int_1^\infty\frac{dx}{x}\left(\frac{x}{x+1/k}-1\right)=-\ln\left(1+\frac{1}{k}\right). \tag{B3}$$

Inserting (B3) into (B2) gives the result shown in Eq. (35),

$$S_q\to\ln\left(\frac{(q+2d)^{1/2}+(1+2d)^{1/2}}{(q+2d)^{1/2}+(2d)^{1/2}}\right). \tag{B4}$$

[1] P. C. Stangeby and G. M. McCracken, Nucl. Fusion **30**, 1225 (1990).
[2] F. L. Hinton and R. D. Hazeltine, Phys. Fluids **17**, 2236 (1974).
[3] P. J. Catto and R. D. Hazeltine, Phys. Plasmas **1**, 1882 (1994).
[4] P. Helander and P. J. Catto, Phys. Plasmas **1**, 2213 (1994).
[5] R. D. Hazeltine and P. J. Catto, "Electron physics and ambipolarity in the tokamak scrape-off layer," submitted to Phys. Plasmas.
[6] D. E. Baldwin, J. G. Cordey, and C. J. H. Watson, Nucl. Fusion **12**, 307 (1972).
[7] B. J. Braams, M. F. A. Harrison, E. S. Hotston, and J. G. Morgan, in *Plasma Physics and Controlled Nuclear Fusion Research, 1984* (International Atomic Energy Agency, Vienna, 1985), Vol. 2, p. 125.
[8] Wolfram Research, Inc., *Mathematica*, Version 2.2 (Wolfram Research, Inc., Champaign, Illinois, 1993).
[9] W. Magnus, F. Oberhettinger, and R. P. Soni, *Formulas and Theorems for the Special Functions of Mathematical Physics*, 3rd ed. (Springer-Verlag, New York, 1966), pp. 19–22 and 32–34.

Downloaded 31 Oct 2012 to 194.81.223.66. Redistribution subject to AIP license or copyright; see http://pop.aip.org/about/rights_and_permissions